Combined Photonic-Plasmonic Modes Inside Photonic Crystal Cavities

Abdelali Mrabti[1] · Said El-Jallal[1] · Gaëtan Lévêque[1] · Abdellatif Akjouj[1] ·
Yan Pennec[1] · Bahram Djafari-Rouhani[1]

Abstract In this article, we present a numerical study of the optical properties of a metal nanowire interacting with a localized cavity in a 2D photonic crystal. The nature of the modes, their wavelength and width are investigated as a function of the nanowire's radius. It is shown in particular that a nanowire with diameter about the lattice constant presents very narrow resonances corresponding to hybrid photonic-plasmonic modes, where increased lifetime is attributed to the decrease of the radiative losses by interaction with the photonic crystal. These results open interesting applications in areas where narrow plasmonic resonances are required, as in localized surface plasmon (LSP) resonance-based biosensing.

Localized surface plasmons (LSPs) are optical modes supported by metal nanoparticles, which result from the resonant coupling between the oscillating surface charge created along the particle's surface by an incident electromagnetic field and the light wave that it scatters [1]. For a specific wavelength, depending on the particle shape, volume, material, as well as the optical characteristics of its environment, the extinction cross-section increases and the intensity of light can be enhanced by several orders of magnitude in a length range around the particle well below the wavelength of the incident light [2]. For all of these properties, LSPs are investigated due to both fundamental aspects and applications into numerous domains like biosensing [3–5], surface enhanced Raman spectroscopy [6], photo-thermal therapy [7] or metamaterials and optical cloaking [8]. In a number of applications, it is required to have a resonance as narrow as possible, for example, in biosensing where the principle is to detect a small shift in the resonance wavelength when a target molecule is adsorbed on a metal nanoparticle surface: the resonance width determines the resolution of the sensor and is often the main limitation in LSP resonance-based sensing [9]. As the width of the plasmon resonance is determined by ohmic (which cannot be suppressed) and radiative losses, the narrowest resonances are obtained with the so-called "dark" plasmons modes: the distribution of electric charges on the particle surface is such as the particle does not possess any net dipole, and the radiative waves are cancelled out [10, 11]. Narrow plasmon resonances can be obtained as well by tailoring the environment of the particle, for example, by making it interact with photonic crystals (PCs), as these structures present forbidden bands for radiative waves, which can be tuned by playing with their geometrical parameters. Recently, Solano and co-workers have shown [12, 13] that the absorbance of coated gold nanospheres and nanorods could be tailored when placed in a defect layer of a multilayer planar resonator: enhancement of the absorption takes place within the band-gap at wavelengths close to the one of the cavity defect and narrowing of the resonance results from the filtering of light by the cavity mode. Following that work, Wang et al. [14] have shown theoretically that the same system could show greatly enhanced photo-induced change of the optical transmittance based on the modification of the dielectric function of the

✉ Gaëtan Lévêque
gaetan.leveque@univ-lille1.fr

[1] Institut d'Electronique, de Microélectronique et de Nanotechnologie UMR CNRS 8520, Villeneuve d'Ascq, France

gold nanoparticles on a subpicosecond time scale with an ultrashort light pulse. In that perspective, increasing the confinement of the localized plasmon mode of a nanoparticle using 2D photonic crystal is of great interest for novel photonic devices. Hence, we propose in this article a detailed study of a 2D photonic crystal interacting with an arbitrary size 2D metal nanoparticle.

More precisely, we investigate in this article the optical properties of an infinitely long nanowire (NW) with circular cross-section, placed inside a localized cavity of a photonic crystal (Fig. 1). We aim at characterizing the optical modes of that system, by their nature, wavelength and resonance width, together with their electromagnetic field distribution. The geometrical parameters of the photonic crystal have been chosen in order to have the localized plasmon wavelengths of the NW within the band gap of the PC. We expect that the radiative contribution to damping rate will be strongly modified as the radiative waves emitted by the NW at the resonance are prevented from leaking inside the PC. The PC is made of a square grating of 2D circular air holes of radius r and lattice parameter a, embedded inside a dielectric matrix with large refractive index, equal to 2.9 in the following. That high value allows ensuring a large index contrast between the material and the air holes, which allows obtaining large and deep band gaps, that could not be reached with lower index materials like SiO_2. The metal NW is a cylinder of radius R made of gold and is placed at the centre of a localized cavity obtained by filling an air hole with dielectric. The moderate value chosen for the refractive index allows keeping the surface plasmon wavelengths of the NW in the visible range. The data for the dielectric constant of gold are extracted from Johnson and Christy [15],
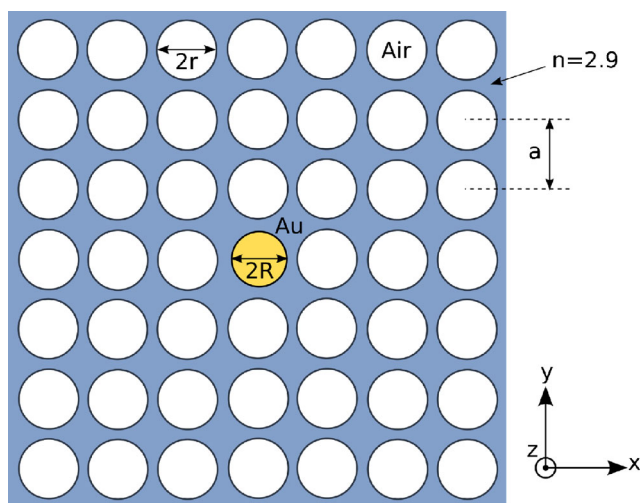

Fig. 1 The investigated structure is a square photonic crystal with lattice parameter a, made of air holes with radius r inside a dielectric matrix with refractive index $n = 2.9$, where one of the hole is replaced by a metal NW of varying radius R

and the calculations were performed using finite element methods (COMSOL Multiphysics, radio-frequency module). In the first part, we present the properties of the gold NW embedded in the homogeneous dielectric medium. In parallel, we show the band gap-tuning properties of the photonic crystal as a function of the grating filling factor, together with the calculation of the photonic modes sustained by the localized cavity. In the second part, we present how both the photonic modes of the PC and the NW's plasmonic modes are affected when the metal NW is placed inside the cavity. The results are discussed as a function of the radius of the gold NW, first when it is much lower than the grating's period and second when both the radius and the period have similar values.

Optical Properties of the Metal NW and the Uncoupled PC

Au NW Inside the Homogeneous and Infinite Dielectric Medium

Figure 2 shows the extinction and absorption spectra of the gold NW in the homogeneous dielectric matrix as a function of its radius R. The NW have several high-order plasmon resonances which have their largest extinction signature between 600 and 700 nm. The resonances are labelled by their order m, $m = 1$ corresponding to the dipolar mode, $m = 2$ to the quadrupolar mode and so on. As the refractive index of the embedding medium is quite high compared to more usual materials in plasmonics, like silica or water, the LSP modes supported by the NW can have a large order m, up to $m = 7$ for the 150-nm radius NW. The quadrupolar mode appears in the visible range of wavelengths for a diameter of about 40 nm, for which the dipolar resonance is redshifted and barely noticeable. The absorption map (Fig. 2b) is quite different from the extinction map (Fig. 2a), due to the fact that the contribution of the scattering to the extinction increases with the NW size. As can be seen on Fig. 3, the absorption is comparable to the scattering for a small NW of radius about 10 nm, but as the NW is rapidly large compared to the wavelength of the light in the medium (far from the electrostatic approximation), the scattering largely dominates when the NW diameter increases, as it can be verified for $R = 85$ nm. This is the reason why in Fig. 2 the extinction is high for larger radii, while the absorption appears low.

Photonic Crystal

The geometrical parameters of the photonic crystal have been chosen in order to tune its absolute band gap to the 600/700-nm wavelength domain, where the NW's LSP
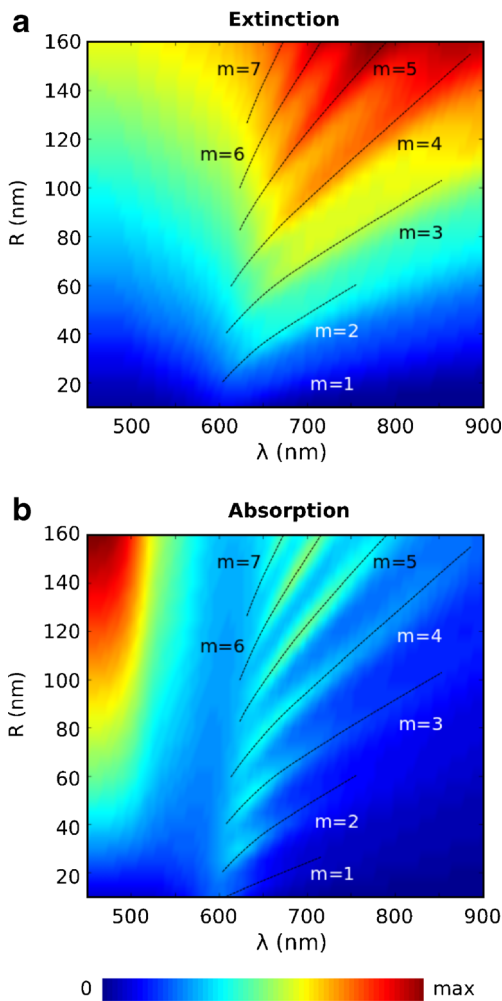
Fig. 2 Extinction (**a**) and absorption (**b**) plotted as a function of the wavelength and the NW's radius (arbitrary units, maximum in *red*, minimum in *blue*). The labels *m* indicate the order of the different localized plasmon mode
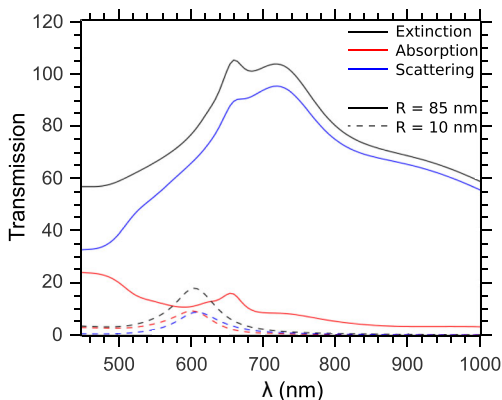

Fig. 3 Comparison between the extinction (*black*), absorption (*red*) and scattering (*blue*) cross-sections for a NW of radius $R = 10$ nm (*dashed line*) and a NW of radius $R = 85$ nm (*solid line*)

modes are the most efficiently excited. As the refractive index is fixed, the only two degrees of freedom are the period a of the grating and the radius r of the air hole, which both allow to change the central wavelength, the width and the depth of the band gap. We have fixed the period to $a = 320$ nm, while Fig. 4a shows the evolution with r/a of the transmission spectra of a plane wave in normal incidence onto one of the (10) direction of the grating, limited to seven lines of holes. The polarization of the incident wave is TM, the incident magnetic field being along the invariance direction. In this transmission calculations and the following, periodic boundary conditions have been applied in the x-direction, while perfectly matched layers have been applied in the incidence and emergence media, perpendicular to the incident plane wave direction. The transmission spectrum has been computed by integrating the Poynting vector flow through a line parallel to the PC in the emergence medium.
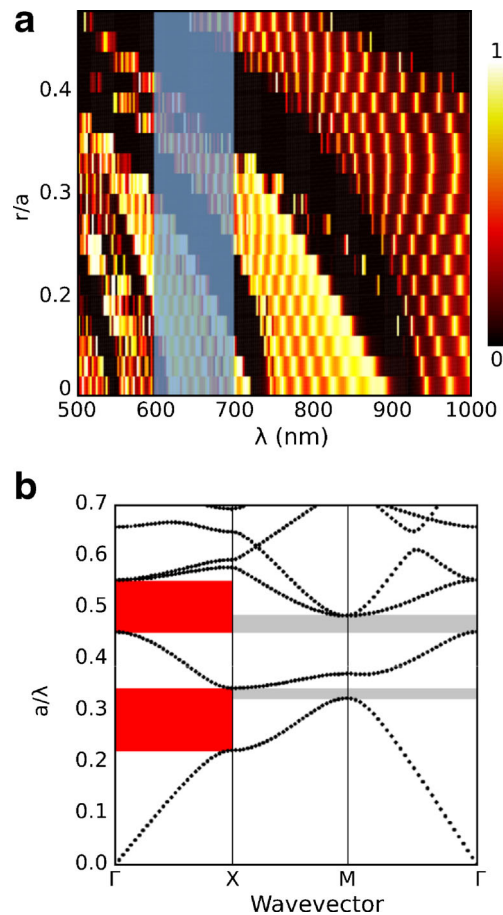

Fig. 4 **a** Transmission of a TM-plane wave in normal incidence on a PC made of seven lines of air holes with radius r and period $a = 320$ nm, as a function of r/a. Maximum transmission is *white*, minimum is *black*; **b** Band diagram of the PC along the high symmetry axes ΓX, XM and $M\Gamma$ of the first Brillouin zone, with period $a = 320$ nm and $r/a = 0.42$. The *grey areas* represent the absolute band gap, whereas the *red areas* represent the band gap in the ΓX direction

It appears that the structure supports several band gaps and that for $R/a \approx 0.42$, a large band gap overlaps with the target wavelength domain (blue area). In order to check the consistency of the transmission calculations, we have compared these results with a full modal dispersion calculation, as shown in Fig. 4b, for $a = 320$ nm and $r = 0.42a$. We can see that a complete band gap exists in the reduced frequency domain $a/\lambda \in [0.4524; 0.4841]$ ($\lambda \in [661$ nm; 707 nm] with $a = 320$ nm), whereas a partial band gap in the ΓX direction exists in the interval $a/\lambda \in [0.452; 0.554]$ ($\lambda \in [578$ nm; 707 nm] with $a = 320$ nm).

A cavity is then created by filling one of the air holes with dielectric. On Fig. 5a, the dispersion calculation on a 7×7 supercell shows that two localized photonic modes,

respectively (a) and (s), are found inside the complete band gap for reduced frequencies a/λ respectively equal to 0.48 ($\lambda = 668$ nm) and 0.46 ($\lambda = 694$ nm). The distribution of the electric field amplitude is shown on the colormaps, Fig. 5a, right. The lowest wavelength mode (a) has an annular shape; its field lines form closed loops around the centre of the cavity where the intensity reaches a minimum. We can notice that the mode is antisymmetric with respect to the two principal axes of the photonic crystal cavity. The highest wavelength mode (s) has a very different distribution of electric field and shows several local maxima inside the cavity. It is symmetric with respect to the main axes of the photonic crystal cavity and reaches as well a minimum amplitude at the centre of the cavity. Figure 5b shows the transmission spectra of a TM-plane wave normally incident on the (10) direction of the grating, still limited to seven rows. The wavelength and electric field distribution of the main resonance is consistent with the ring mode (a) found with the dispersion calculation. The mode at 694 nm is not excited because as the incident light is normally incident onto the photonic crystal, it is antisymmetric with respect to the vertical direction and cannot couple to the 694-nm symmetric mode. However, the same calculation performed with a small incidence angle breaks the symmetry of the incident field and allows to recover the corresponding transmission peak (not shown) at the wavelength predicted by the dispersion calculation.

Coupled Systems

In this section, we investigate the optical behaviour of the gold NW placed at the centre of the localized PC cavity. The absorption spectra have been calculated as a function of the NW radius, by integration of the power losses on the cross section of the NW, and normalization to the incident energy flow on the 7×7 supercell. Hence, reflection (R), transmission (T) and absorption (A) obey the energy conservation $R + T + A = 1$. Two very different behaviours have been obtained, according to the radius of the NW compared to the grating's period.

Case Where $R \ll a$

We consider first the case where the NW has a radius R small compared to the lattice parameter a. Figure 6 shows the evolution of the transmission peak of the ring mode (a), from radius 10 to 50 nm. The wavelength of the mode is blueshifted when R increases, while its transmission rapidly decreases. For comparison, the absorption spectra have been added, which shows that both absorption and transmission reach comparable low values and that most of the
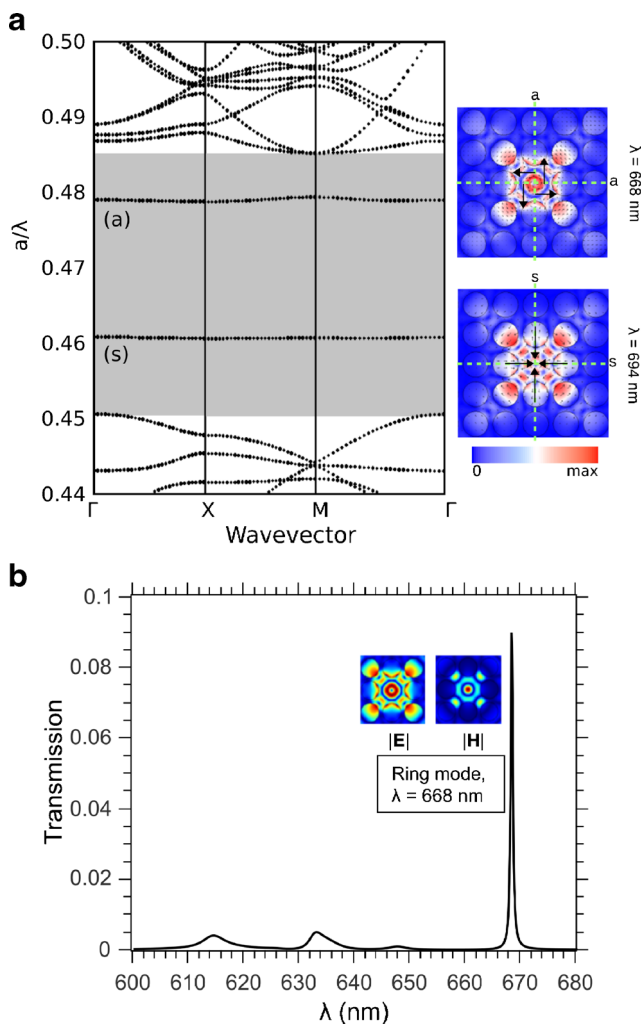
Fig. 5 **a** Band diagram of the 7×7 supercell of the same PC with a localized cavity. The wavelength and electric field distributions have been indicated for $a = 320$ nm; **b** Transmission of a TM-plane wave in normal incidence on the same PC, limited to seven lines along the direction of the incident wave. The colormaps show the distribution of the amplitude of the electric field, in arbitrary units (*dark blue* is zero, *red* is the highest value.)
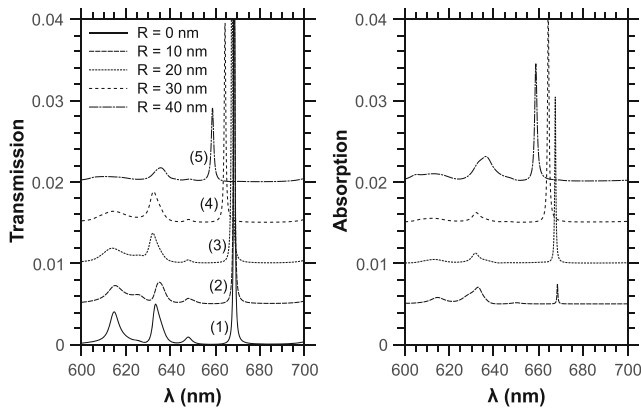
Fig. 6 Transmission and absorption spectra of the system composed of the gold NW of radius R placed at the centre of the cavity, for wavelengths close to the cavity ring mode position. For readibility purposes, spectra have been shifted by 0.005 per radius increment. Maxima of transmission (absorption) are 8.5 (0.24) % (R = 10 nm), 6.0 (2.0) % (R = 20 nm), 2.5 (2.6) % (R = 30 nm) and 0.9 (1.5) % (R = 40 nm)

energy is then reflected. Table 1 shows the different resonant wavelengths, together with the electric and magnetic field intensity distribution for $R \leq 40$ nm. It appears that the particular ring structure of the unperturbed PC cavity modes persists for values of R up to few nanometers. Indeed, as the intensity of the PC cavity ring mode is almost zero at the centre, its shape and wavelength is unchanged in the limit of very small NW ($R = 10$ nm). However, when R increases, we can intuitively understand the decrease of the mode wavelength by the fact that the light is pushed away from the area occupied by the metal NW: this leads to a decrease of the area accessible to the photonic mode and then a shortening of the resonance wavelength.

Moreover, if the shape of the mode is unchanged for small radius, it is not the case for a NW radius larger than 50 nm, where the light ring is much closer to the adjacent air holes. This breaks the revolution symmetry of the ring

Table 1 Summary of the wavelengths and field distributions for the different peaks labelled (1) to (5) on Fig. 5. On colormaps, dark blue is zero and red is the highest value of the electric/magnetic field's amplitude

	R(nm)	$|\mathbf{E}|$	$|\mathbf{H}|$	λ (nm)
(1)	0			668.6
(2)	10			668.5
(3)	20			667.6
(4)	30			664.5
(5)	40			658.9

mode, and for $R > 50$ nm, the ring mode does not exists anymore. Finally, let us emphasize that this mode, when the NW radius is much smaller than the lattice constant, is purely photonics, without plasmonic characteristics, as the electric field is, in every point of the metal interface, parallel to it, and then cannot create the surface charge necessary to excite surface plasmon waves.

Case Where 2R is Comparable to a

The opposite regime is when the NW diameter is comparable to the lattice parameter. In that case, the light is squeezed in the very narrow space in between the gold interface and the air holes, and strong coupling occurs between the gold NW and the photonic crystal.

Figure 7 shows the evolution of the transmission and absorption spectra for NW radius varying from 100 to 150 nm. Maximum values, indicated in the caption, show that the incident energy is mostly reflected, but a significant part is absorbed (up to 14 % for R = 120 nm) whereas less than 1 % is transmitted. This is a very different behaviour than for small radius, where both maximal absorption and transmission are of the same order of magnitude. For R between 100 and 130 nm, only one mode is excited between 600 and 700 nm, labelled (1). It is redshifted with R until $R = 110$ nm, while for larger radius, it blueshifts. Similarly, a second peak, labelled (2), appears for $R = 140$ nm at a wavelength of about 660 nm and is blueshifted with R. This blueshift of these two modes with large values of R might be surprising as the localized plasmon modes of a single NW usually shift to the red with diameter (see Fig. 1). This is actually what is observed when $R < 110$ nm. When
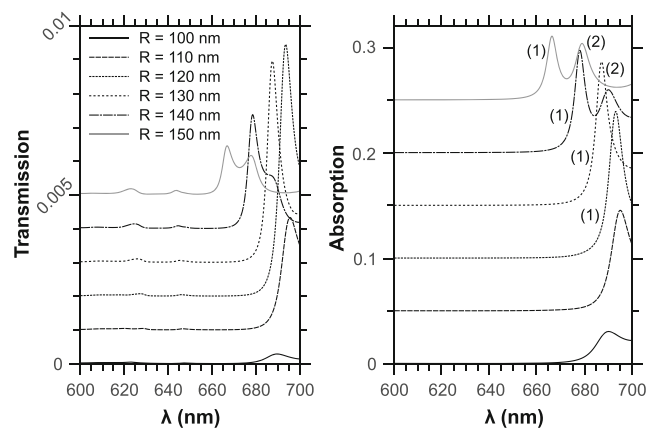

Fig. 7 Transmission and absorption spectra of the coupled system with the NW's radius R comparable to the grating's period a. For readability purpose, spectra have been shifted by 0.001 per radius increment for transmission and 0.5 per radius increment for absorption. Maxima of transmission(absorption) are 0.03 (3.0) % (R = 100 nm), 0.33 (9.5) % (R = 110 nm), 0.75 (13.9) % (R = 120 nm), 0.60 (13.6) % (R = 130 nm), 0.34 (9.7) % (R = 140 nm) and 0.15 (6.1) % (R = 150 nm)

R becomes larger, the reversed evolution of the wavelength can be explained by the decrease of the effective refractive index surrounding the NW: for wider NW, the air holes are closer to the wire's edges and the portion of low refractive index (air holes) in the area occupied by the optical mode is larger. In that case, the blueshift due to the lowering refractive index is larger than the redshift due to the increasing diameter.

The distribution of the electric and magnetic field amplitude together with surface charges (plotted at the time of maximal amplitude) is displayed on Table 2 for the modes (1) and (2) and $R = 150$ nm. In both cases, the distribution of the electric field looks complex and difficult to interpret. However, the magnetic field structure is much simpler and shows clearly a similarity between the mode (1) and the octupolar mode ($m = 4$) of the single NW in the homogeneous dielectric matrix: the main qualitative difference is at the proximity of the air holes where one intensity maxima out of two around the NW is lower than its nearest neighbours. The similarity with the octupolar mode is confirmed by the repartition of the surface charges which clearly demonstrates that this mode is antisymmetric with respect to the two principal axis of the photonic crystal.

The mode (2) has a very different structure as indicated by the magnetic field distribution, as the maxima around the NW surface are evenly distributed, except on the axis perpendicular to the excitation direction where the light intensity is zero. This can be understood by the surface charges distribution which is antisymmetric compared to the vertical main axis, whereas it is symmetric compared to the horizontal axis. This results in a zero of field along the NW's horizontal diameter. This last mode is clearly different from the single NW modes and as a direct consequence results intrinsically from the coupling of the localized plasmon of the NW with the photonic crystal. As both modes (1) and (2) result from the strong coupling of the NW and the PC, we will call them PC-plasmon modes in the following.

Table 2 Structure of the compounds modes (1) and (2) for $R = 150$ nm. On colormaps, dark blue is zero and red is the highest value of the electric/magnetic field's amplitude. For surface charges distributions, green is zero
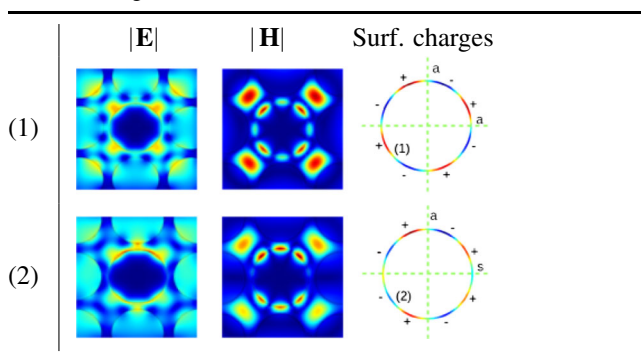
We compare on Fig. 8 the modes (1) and (2) for the $R = 140$-nm NW (a) with the modes of the isolated NW with the same radius in the homogeneous matrix (b). We can clearly see that the PC-plasmon modes are much narrower. More precisely, mode (1) and (2) have a similar full width at half maximum (FWHM) of about 6 nm, which corresponds to a quality factor of 113 for mode (1), whereas the $m = 6$ mode at 680 nm for the isolated NW has a FWHM of 36 nm with a quality factor of 19. This reduction of the mode width by a factor of about 6 is attributed to the lowering of the radiative contribution of the electromagnetic field scattered by the NW at the resonance, which is forbidden to propagate into the photonic crystal. This phenomenon should be responsible for the decreases of the radiative losses, making the plasmon mode width limited principally by its ohmic losses.

Finally, Fig. 9 summarizes the different phenomena involved in the coupling of the metal NW with the photonic crystal for a radius varying between 0 and 150 nm by step of 10 nm, with few representative magnetic field distributions. Transmission and absorption spectra have been plotted side-by-side in log scale. As previously explained, for small radius, the ring mode is not strongly affected by the NW and shifts to the blue (R branch), whereas the PC-plasmon modes (1) and (2) appear for radius larger than 110 nm. In between, we can see one mode which is linearly redshifted with R: it corresponds to the octupolar, $m = 4$, mode of the NW in the homogeneous matrix. The hexapolar $m = 3$ mode appears at $\lambda = 680$ nm for $R = 60$ nm, but shifts beyond 700 nm for larger radius. Actually, for small radius, these modes are not strongly affected by the photonic crystal as the plasmon mode does not strongly overlap with the air holes of the photonic crystal. A transition occurs at
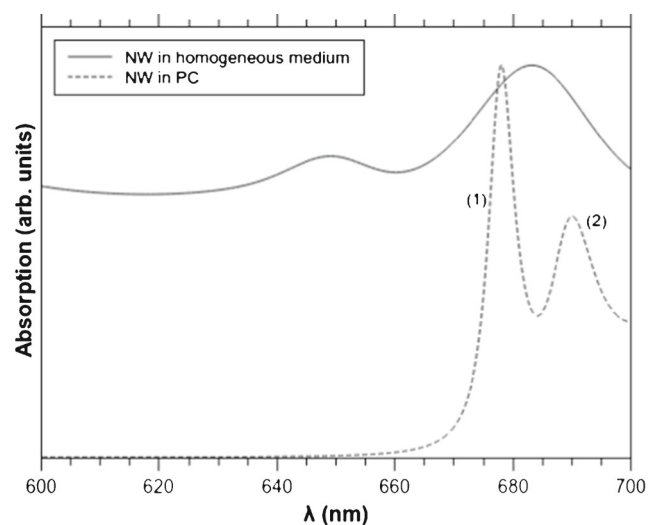

Fig. 8 Comparison between the absorption spectra for the single NW in infinite dielectric medium (a) and the NW of radius 140 nm in the PC cavity
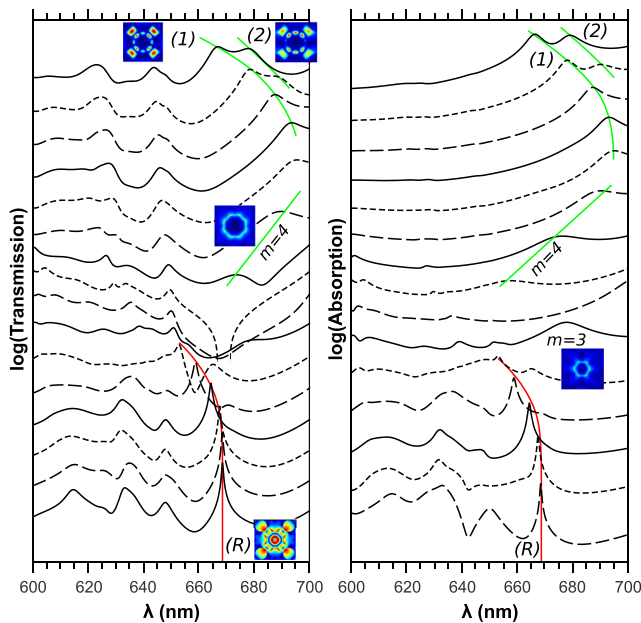
Fig. 9 Evolution of absorption in the metal NW, as a function of the wavelength and the NW radius

about $R = 100$ nm where these modes start to combine with the photonic crystal to give the PC-plasmon modes (1) and (2) previously described, where they show much narrower than modes $m = 3$ and $m = 4$.

Summary

In this work, we have investigated the optical properties of a 2D metal NW placed at the centre of a localized cavity in a 2D photonic crystal. The nature of the modes, their wavelength, together with their evolution with the NW radius is very dependent on how the diameter compares to the grating period. The ring photonic mode of the PC cavity has his shape essentially unaffected by a NW of few 10-nm diameter, while its wavelength blueshifts. However, for a NW with diameter about the lattice constant, the coupled system present very narrow resonances corresponding to compound PC-plasmon modes, where the narrowing of the resonance is attributed to the decay of the radiative losses of the plasmon mode by the photonic crystal. These results open interesting applications in areas where tailoring the plasmon response of a nanoparticle is required, as in LSP resonance biosensing or high-speed photonic devices. A biosensor could be obtained in this geometry, for example, by filling one or several of the eight nearest holes from the NW with a fluid to probe. Otherwise, alternative configurations working on this principle could be obtained by creating the photonic crystal inside a thin membrane, the nanoparticle being either incorporated in (in that case close to one of

the membrane's interfaces) or deposited on the membrane, in contact with the medium under sensing. Besides, such a system is a choice platform for investigating the coupling of localized plasmon modes with elastic waves, as it has previously been demonstrated that PC can lead to enhanced interaction between phononic and photonic waves [16, 17]. Similarly, such a compound photonic crystal/metal particle system could show enhanced interaction between elastic and plasmonic waves [18–20], allowing to achieve mechanical control of the plasmon response at a sub-micrometre scale.

References

1. Stefan a Maier (2007) Plasmonics: fundamentals and applications. Springer US, Boston, MA
2. Kottmann JP, Martin OJF, Smith DR, Sheldon S (2001) Dramatic localized electromagnetic enhancement in plasmon resonant nanowires. Chem Phys Lett 341(1-2):1–6
3. Mock JJ, Smith DR, Schultz S (2003) Local refractive index dependence of plasmon resonance spectra from individual nanoparticles. Nano Lett 3(4):485–491
4. Saison-Francioso OlO, Leveque G, Akjouj A, Pennec Y, Djafari-Rouhani B, Szunerits S, Boukherroub R, Gaetan Lévêque (2012) Plasmonic nanoparticles array for high-sensitivity sensing: a theoretical investigation. Jo Phys Chem C 116(33):17819–17827
5. Maurer T, Nicolas R, Lévêque G, Subramanian P, Proust J, Béal J, Schuermans S, Vilcot J-P, Herro Z, Kazan M, Plain J, Boukherroub R, Akjouj A, Djafari-Rouhani B, Adam P-M, Szunerits S (2013) Enhancing LSPR ensitivity of Au gratings through graphene coupling to Au film. Plasmonics 9(3):507–512
6. Wen X, Li Guangyuan, Zhang Jun, Zhang Qing, Peng Bo, Wong LaiMun, Wang Shijie, Xiong Q (2014) Transparent free-standing metamaterials and their applications in surface-enhanced Raman scattering. Nanoscale 6(1):132–139
7. Jaque D, Martínez Maestro L, Del Rosal B, Haro-Gonzalez P, Benayas A, Plaza JL, Martín Rodríguez E, García Solé J (2014) Nanoparticles for photothermal therapies. Nanoscale 6(16):9494–9530
8. Liu S-D, Yang Z, Liu R-P, Li X-Y (2011) Plasmonic-induced optical transparency in the near-infrared and visible range with double split nanoring cavity
9. Mayer KM, Hafner JH (2011) Localized surface plasmon resonance sensors. Chem Rev 111(6):3828–3857
10. Schmidt F-Ph, Ditlbacher H, Hohenester U, Hohenau A, Hofer F, Krenn JR (2012) Dark plasmonic breathing modes in silver nanodisks. Nano Lett 12(11):5780–5783
11. Verellen N, Dorpe PV, Huang C, Lodewijks K, Vandenbosch GAE, Lagae L, Moshchalkov VV (2011) Plasmon line shaping using nanocrosses for high sensitivity localized surface plasmon resonance sensing. Nano Lett 11:391–397
12. Sánchez-Sobrado O, Lozano G, Calvo ME, Sánchez-Iglesias A, Liz-Marzán LM, Míguez H (2011) Interplay of resonant cavity modes with localized surface plasmons: optical absorption properties of Bragg stacks integrating gold nanoparticles. Adv Mater (Deerfield Beach, Fla.) 23(18):2108–2112
13. Jiménez-Solano A, López-López C, Sánchez-Sobrado O, Luque JM, Calvo ME, Fernández-López C, Sánchez-Iglesias A, Liz-Marzán LM, Míguez H (2012) Integration of gold nanoparticles in optical resonators. Langmuir: ACS J Surf Colloids 28 (24):9161–9167

14. Wang X, Palpant B (2013) Large and ultrafast optical response of a one-dimensional plasmonic–photonic cavity. Plasmonics 8(4):1647–1653

15. Johnson PB, Christy RW (1972) Optical constants of the noble metals. Phys Rev B 6(12):4370–4379

16. Rolland Q, Oudich M, El-Jallal S, Dupont S, Pennec Y, Gazalet J, Kastelik JC, Lévêque G, Djafari-Rouhani B (2012) Acousto-optic couplings in two-dimensional phoxonic crystal cavities. Applied Physics Letters 101(6):061109

17. El-Jallal S, Oudich M, Pennec Y, Djafari-Rouhani B, Makhoute A, Rolland Q, Dupont S, Gazalet J (2014) Optomechanical inter-actions in two-dimensional Si and GaAs phoXonic cavities. J Phys Condens Matter: Inst Phys J 26(1):015005

18. Large N, Saviot L, Margueritat J, Gonzalo J, Afonso CN, Arbouet A, Langot P, Mlayah A, Aizpurua J (2009) Acousto-plasmonic hot spots in metallic nano-objects. Nano Lett 9(11):3732–3738

19. Kelf Ta, Hoshii W, Otsuka PH, Sakuma H, Veres Ia, Cole RM, Mahajan S, Baumberg JJ, Tomoda M, Matsuda O, Wright OB (2013) Mapping gigahertz vibrations in a plasmonic-phononic crystal. New J Phys 15(2):023013

20. Tripathy S, Marty R, Lin VK, Teo SL, Ye E, Arbouet A, Saviot L, Girard C, Han MY, Mlayah A (2011) Acousto-plasmonic and surface-enhanced Raman scattering properties of coupled gold nanospheres/nanodisk trimers. Nano Lett 11(2):431–437